Interfacial fluid transport is a key to hydrogel bioadhesion

Raphaël Michel[a,b,1], Léna Poirier[a], Quentin van Poelvoorde[a], Josette Legagneux[c], Mathieu Manassero[d,e], and Laurent Corté[a,b,1]

[a]Ecole Supérieure de Physique et Chimie Industrielle de la Ville de Paris (ESPCI Paris), Paris Sciences et Lettres Research University, Laboratoire Matière Molle et Chimie, CNRS UMR 7167, 75005 Paris, France; [b]MINES ParisTech, Paris Sciences et Lettres Research University, Centre des Matériaux, CNRS UMR 7633, 91003 Evry, France; [c]Ecole de Chirurgie, Agence Générale des Équipements et Produits de Santé, Assistance Publique-Hôpitaux de Paris, 75005 Paris, France; [d]Service de Chirurgie, Ecole Nationale Vétérinaire d'Alfort, 94700 Maisons-Alfort, France; and [e]Laboratoire de Bioingénierie et Bioimagerie Ostéo-Articulaire, CNRS UMR 7052, 75010 Paris, France

Edited by David A. Weitz, Harvard University, Cambridge, MA, and approved December 3, 2018 (received for review August 3, 2018)

Attaching hydrogels to soft internal tissues is a key to the development of a number of biomedical devices. Nevertheless, the wet nature of hydrogels and tissues renders this adhesion most difficult to achieve and control. Here, we show that the transport of fluids across hydrogel–tissue interfaces plays a central role in adhesion. Using ex vivo peeling experiments on porcine liver, we characterized the adhesion between model hydrogel membranes and the liver capsule and parenchyma. By varying the contact time, the tissue hydration, and the swelling ratio of the hydrogel membrane, a transition between two peeling regimes is found: a lubricated regime where a liquid layer wets the interface, yielding low adhesion energies (0.1 J/m^2 to 1 J/m^2), and an adhesive regime with a solid binding between hydrogel and tissues and higher adhesion energies (1 J/m^2 to 10 J/m^2). We show that this transition corresponds to a draining of the interface inducing a local dehydration of the tissues, which become intrinsically adhesive. A simple model taking into account the microanatomy of tissues captures the transition for both the liver capsule and parenchyma. In vivo experiments demonstrate that this effect still holds on actively hydrated tissues like the liver capsule and show that adhesion can be strongly enhanced when using superabsorbent hydrogel meshes. These results shed light on the design of predictive bioadhesion tests as well as on the development of improved bioadhesive strategies exploiting interfacial fluid transport.

bioadhesion | hydrogel | interface | transport | liver

Hydrogels are essential components of implants and surgical devices, used as protective layers (1), sealants (2), platforms for drug or cell delivery (3), or substrates for biosensors (4). These applications require that hydrogels be secured on the soft and wet tissues of internal organs. Fixation by mechanical fasteners like sutures is most often not satisfactory, as it damages both tissues and hydrogels (5). Much more appropriate fixation methods are sutureless approaches producing an intimate and adhesive contact at the interface between hydrogels and tissues (6). In recent years, major progress has been made to create bioadhesive hydrogel surfaces by introducing binding interactions between hydrogel networks and biological tissues through surface functionalization (7–9), mechanical interlocking (10), or coating with nanoparticles (11). Nevertheless, the design of such bioadhesive hydrogels is greatly challenged by the wet conditions of the interface (12). Tissue surfaces are continuously perfused by vascular flows and hydrated by surrounding biological fluids, which hinders the contact between hydrogels and tissues and compromises the establishment of adhesive binding. Most interestingly, hydrogel formulations are often not swollen to equilibrium at the moment of contact with biological tissues. Therefore, water ought to be transported from the tissue into the hydrogel. Seminal studies on adhesion to mucus membranes have shown that the tissue dehydration resulting from this transport could be a driving mechanism for bioadhesion (13, 14). Adhesion experiments between model hydrogels have confirmed this effect (15, 16). However, the contribution of such interfacial transport to hydrogel–tissue adhesion remains to be elucidated, and its applicability for the design of bioadhesive systems has been very little exploited hitherto. Here, we address this question, using adhesion experiments of model hydrogels on animal tissues.

Our study concentrates on adhesion to the outside and inside tissues of the liver, which is commonly used to assess the performance of bioadhesives (7–9, 17–19). The outer part of the liver, the Glisson's capsule, hereafter referred to as "capsule," is delimited by a membrane constituted of superimposed thin tissue layers (20). Its outermost surface is composed of a monolayer of mesothelial cells attached to a 100-nm-thick basal membrane. These cells produce a liquid coating, the glycocalyx, composed of an aqueous solution of hyaluronan that has both a lubricant and a protective role (20). The inner part of the liver, hereafter referred to as "parenchyma," is a soft porous structure irrigated by a dense network of vessels (21). It is divided into lobules having a characteristic diameter varying from 1 mm to 2.5 mm where the blood is filtered and bile is produced (22). Herein, we use porcine liver, which has an anatomy and hemodynamics that differ little from those of human liver (23).

Model hydrogel membranes were fabricated from poly(ethylene glycol) (PEG) films. Similar PEG hydrogels are used in modern surgery as sealant (2). They are known to adhere to biological tissues due to hydrogen bonding between ether oxygens and the protons of amino and hydroxy groups contained in biomolecules (24, 25) as well as short-range hydrophobic

Significance

Bioadhesive hydrogels capable of sticking to living tissues are of utmost interest for better-integrated implants and less invasive surgical techniques. Nevertheless, adhesion is most difficult to achieve and control on the wet surface of internal tissues. This work demonstrates that fluid transport across the tissue–hydrogel interface governs the creation of adhesion. Through ex vivo experiments and a simple model, we capture how the onset of adhesion depends on a competition between draining and wetting of the interface. This coupling between adhesion and interfacial transport provides a potent key to improve the accuracy of adhesion tests and to enhance the bioadhesive performance of hydrogels. We illustrate this potential in vivo by using superabsorbent hydrogel membranes to make strong liver adhesives.

Author contributions: R.M. and L.C. designed research; R.M., L.P., Q.v.P., J.L., M.M., and L.C. performed research; R.M., L.P., Q.v.P., M.M., and L.C. analyzed data; and R.M., M.M., and L.C. wrote the paper.

The authors declare no conflict of interest.

This article is a PNAS Direct Submission.

[1]To whom correspondence may be addressed. Email: r.michel3@hotmail.fr or laurent.corte@mines-paristech.fr.

This article contains supporting information online at www.pnas.org/lookup/suppl/doi:10.1073/pnas.1813208116/-/DCSupplemental.

Published online January 2, 2019.

interactions with tissue proteins (26), as illustrated in Fig. 1*A*. In this study, smooth 1-mm-thick films having a roughness of less than 1 μm (*SI Appendix*, Fig. S1) were produced from diacrylate telechelic PEG chains (M_n = 700 kg/mol) chemically cross-linked with multifunctional thiols (*SI Appendix*, *SI Materials and Methods*). In water, these films reach equilibrium swelling in 2.5 h (*SI Appendix*, Fig. S2). In the following, hydrogel swelling is characterized by the swelling ratio, Q, defined as the mass of the swollen film over the mass of the dry film. At equilibrium in water, the swelling ratio of the studied PEG films is $Q_{eq} = 2.00 \pm 0.05$, which corresponds to a water content of 50 wt%.

Results and Discussion

Ex Vivo Adhesion Measurements. The adhesion between PEG hydrogels and porcine liver tissues was measured ex vivo using a 90° peeling experiment as depicted in Fig. 1*B*. In each experiment, a 1-cm-thick, 3-cm-wide and 12-cm-long rectangular section of liver was cut and glued onto a flat holder. A 1-cm-wide ribbon of PEG hydrogel was deposited on the liver surface over an 8-cm length (step i). A pressure of 50 kPa to 60 kPa was applied with a finger over the contact area for 1 min to reproduce a surgical deposition (step ii). The ribbon was then left in contact for a given contact time (Δt), after which it was peeled from the liver at a constant 90° angle and a constant speed of 1 mm/s (step iii). The force and displacement measured at the top end of the ribbon were recorded, as well as side and front views of the peeling zone.

Typical peeling force–displacement curves are given in Fig. 1*C* for dry PEG ribbons ($Q = 1$) after a 5-min contact on both the parenchyma and the capsule of freshly dissected livers. Two regimes can be clearly distinguished. In the first regime, adhesion is very weak, with a normalized peeling force in the range 0.5 N/m to 1 N/m. It is illustrated in Fig. 1*C* for the parenchyma (dotted red curve). Observations of the detachment zone show that the interface is lubricated by a liquid layer with a meniscus moving as peeling proceeds (Fig. 1*D* and Movie S1). We refer to this regime as the "lubricated" regime. In the second regime, the normalized peeling force reaches higher values in the 1 N/m to 10 N/m range. It is illustrated in Fig. 1*C* for both the parenchyma (full red curve) and the capsule (full green curve). The liver tissues are deformed and lifted by the gel, as shown in Fig. 1*E* and Movie S2 for the parenchyma and in *SI Appendix*, Fig. S3 and Movie S3 for the capsule. We refer to this regime as the "adhesive" regime. For the parenchyma, this regime even leads to a transfer of tissues to the hydrogel surface, indicating a cohesive rupture in the tissue (*SI Appendix*, Fig. S4).

The interfacial adhesion energy, G, can be calculated from those peeling curves using Kendall's (27) theory of elastic peeling. For 90° peeling, the adhesion energy is simply given by $G = F/w$, where F/w is the mean steady-state value of the peeling force, F, normalized by the ribbon width, w. Adhesion energy for a 5-min contact time with dry PEG ribbons was measured on several liver samples from different animals ($n = 6$) (Fig. 1*F*). For the capsule, all peelings were in the adhesive regime with an adhesion energy of 2.3 ± 0.5 J/m^2, while, for the parenchyma, peeling was either in a lubricated or adhesive regime depending on the liver. In the latter case, the difference in adhesion energy between lubricated (open symbols, $G = 0.9 \pm 0.3$ J/m^2) and adhesive regimes (full symbols, $G = 3.1 \pm 0.3$ J/m^2) is statistically significant ($P < 0.0001$).

The hydrogel–liver adhesion depends on the swelling state of the deposited hydrogels. To show this dependence, PEG ribbons were swollen to different swelling ratios from dry state ($Q = 1$) to equilibrium swelling ($Q_{eq} = 2$). The corresponding adhesion energies are given in Fig. 1*G* for a 5-min contact time on the same liver. Adhesion energy decreases with increasing Q. For the parenchyma of this liver, peeling was always in the lubricated regime. For the capsule, a transition from adhesive to lubricated regime was observed for $Q > 1.2$. Similarly, the effect of contact time was explored by varying Δt from 5 min to 30 min with dry PEG ribbons ($Q = 1$), as shown in Fig. 1*H*. For the capsule, adhesion energy is independent of contact time ($G = 3.7 \pm 0.4$ J/m^2). For the parenchyma, a fourfold increase in adhesion energy was observed between 5 min and 15 min of contact, which corresponds to a transition from lubricated to adhesive peeling. When fully swollen hydrogel ribbons were used instead of dry ones (dotted red line in Fig. 1*H*), a lubricated behavior occurred for all of the studied contact times, and no dependence on Δt was observed.

Influence of Liver Hydration on ex Vivo Adhesion. The weight fraction of water in each liver sample, H, was assessed by measuring the mass of dry extract (see protocol in *SI Appendix*, section 4). For freshly dissected livers ($n = 13$), H ranges from 74.5 wt% to 81.6 wt%, with a mean value of 77.4 ± 1.5 wt%. As a comparison, partially bloodless livers from butcher were also used ($n = 16$). Those drained livers contain much less fluid, with an average water content of 72.2 ± 1.7 wt% (*SI Appendix*, Fig. S5). The adhesion energies of dry PEG ribbons after a 5-min contact time

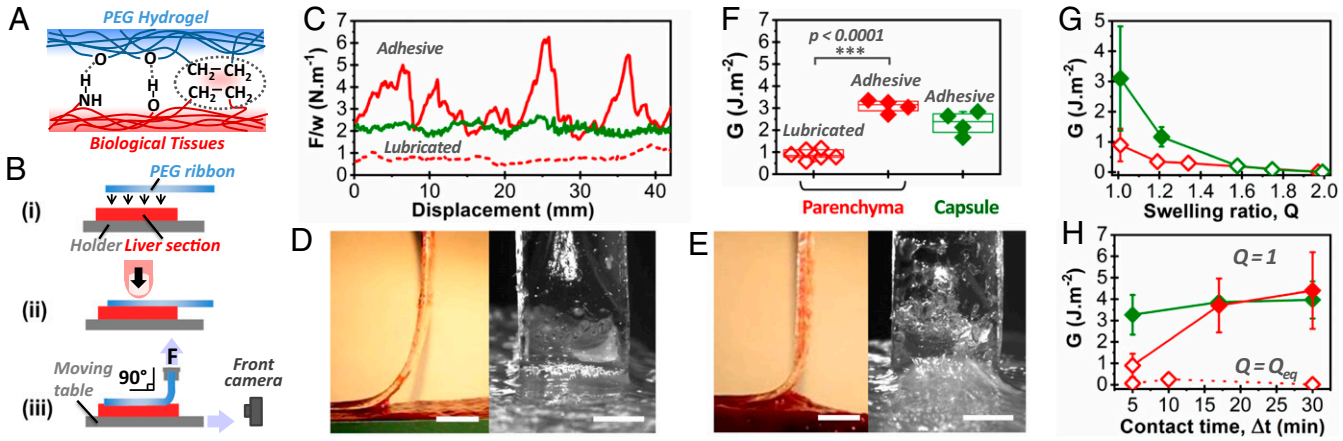

Fig. 1. Ex vivo adhesion on freshly dissected liver tissues. (*A*) Schematic representation of the hydrogen-bonding and hydrophobic interactions between PEG hydrogels and biological tissues. (*B*) Schematic representation of the peeling protocol. (*C*) Normalized peeling force as a function of displacement on the liver capsule (green curve) and parenchyma (red curves) for PEG ribbons ($Q = 1$, $\Delta t = 5$ min). The origin of displacement (0 mm) corresponds to the beginning of the steady-state peeling. (*D* and *E*) Side and front views during peeling of a PEG ribbon ($Q = 1$, $\Delta t = 5$ min) from liver parenchyma displaying (*D*) a lubricated regime or (*E*) an adhesive regime. (Scale bar: 5 mm.) (*F*) Adhesion energy for peeling of PEG ribbons ($Q = 1$, $\Delta t = 5$ min) on liver capsule (green) and parenchyma (red). In this graph and the following, full and open symbols correspond to adhesive and lubricated behaviors, respectively. (*G*) Adhesion energy as a function of hydrogel swelling ratio for $\Delta t = 5$ min: liver capsule (green) and parenchyma (red). (*H*) Adhesion energy as a function of contact time for dry PEG ribbons ($Q = 1$): liver capsule (green) and parenchyma (red). Dotted line shows data for fully swollen PEG ribbons ($Q = Q_{eq}$).

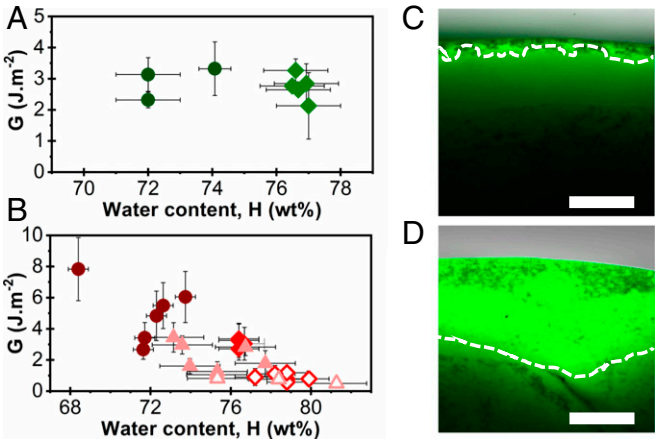

Fig. 2. Influence of liver hydration on ex vivo adhesion. (*A* and *B*) Adhesion energy as a function of liver water content for peeling of PEG ribbons ($Q = 1$, $\Delta t = 5$ min) on (*A*) the capsule and (*B*) the parenchyma of freshly dissected (diamonds) and drained (circles) livers. For the parenchyma, data on rehydrated samples are also represented (triangles). Full and open symbols correspond to adhesive and lubricated peeling, respectively. (*C* and *D*) Fluorescent micrographs of cross-sections of (*C*) a liver capsule and (*D*) a liver parenchyma after 20 min of immersion in physiological serum containing sodium fluorescein (0.1 g/L). Tissue surface is on top. Dashed lines are iso-intensity lines (50% maximum intensity) indicating penetration depth. (Scale bar: 300 μm.)

on the capsule and parenchyma of those livers are plotted in Fig. 2 *A* and *B* as a function of liver water content. For the capsule, the peeling regime was always adhesive, showing no significant dependence on H. For the parenchyma, however, the adhesion energy was found to decrease strongly with H, and a transition from adhesive (full symbols) to lubricated regimes (open symbols) was observed near $H = 77$ wt%.

The relationship between tissue hydration and hydrogel bioadhesion was further confirmed by modulating the hydration of drained livers. For that, liver samples were immersed in physiological serum before peeling. Microscopic observations of liver cross-sections after immersion in serum containing a fluorescent dye showed that tissue rehydration depends on the nature of the tissue surface. For the capsule (Fig. 2*C*), tissue rehydration was hardly noticed and confined to the very surface, due to the barrier property of the basal membrane. This impermeable separation may explain why the adhesion to the capsule is independent of the hydration of underlying tissues. Conversely, for the parenchyma, water penetrated inside the tissues but remained within a superficial layer of ∼1 mm depth (Fig. 2*D*). This localized swelling is explained by the dense collagen-rich walls, which prevent fluid exchanges between lobules. After immersion, the water content at the surface of parenchyma could thus be assessed by considering that the water uptake is contained in the first lobular layer (see calculation in *SI Appendix*, section 4). By varying the immersion time between 0 min and 300 min, the tissue water content near the surface was tuned from 72.9 wt% to 81.5 wt% (*SI Appendix*, Fig. S6). The adhesion energies measured by peeling dry PEG ribbons after 5 min on those rehydrated parenchyma are reported in Fig. 2*B*. We find that fresh and rehydrated tissues having similar hydration levels produce similar adhesion energies. In particular, a transition from lubricated to adhesive regimes was reproduced with rehydrated livers for superficial water content of $H = 77 \pm 2$ wt%. Comparable dependences on Δt and Q were found for drained, rehydrated, and freshly dissected livers (*SI Appendix*, Fig. S7).

Fluid Transport Across the Tissue–Hydrogel Interface. Fluid exchanges across the liver–hydrogel interface were characterized by measuring the water uptake of hydrogel films as a function of contact time. For that, dry PEG films were deposited on the capsule and parenchyma of a freshly dissected liver as depicted in Fig. 3 *A*, *i* and *ii* and weighed after different contact times. These experiments were compared with a control experiment (Fig. 3 *A*, *iii*) where PEG films were deposited on a floating grid with one face in direct contact with a water reservoir. Fig. 3*B* shows the swelling ratio of the films as a function of contact time. In the control experiment, the swelling kinetics is well described by the diffusive relaxation of a hydrogel network (28). Eventually, equilibrium swelling was reached, after 5 h. In the experiments on the liver, fluid was clearly transported from the tissues into the hydrogels. However, for both the capsule and the parenchyma, the swelling ratio converged at long contact times toward a value of $Q = 1.70 \pm 0.05$, well below equilibrium. Swelling was limited by the slow extraction of water from the liver, which suggests that tissue dehydration occurred near the interface. Interestingly, swelling kinetics differ for the capsule and the parenchyma at early contact times. On the capsule, the slow swelling kinetics was observed even for the first minute of contact. On the parenchyma, it only established after 20 min. Before that, the films were swelling as if they were in contact with a water reservoir. This indicates that a finite amount of fluid is quickly transported from the parenchyma to wet the interface.

Effect of Dehydration on Tissue Adhesive Properties. The effect of tissue dehydration on bioadhesion was investigated by comparing the adhesive properties of liver tissues before and after dehydration by a PEG film. For that, liver surfaces were probed by peeling thin ribbons made of polyethylene, which, unlike PEG, is not swollen by water and has no strong binding affinities with biological tissues. For freshly dissected liver surfaces, polyethylene ribbons are poorly adhesive, with adhesion energies of 0.08 ± 0.04 J/m^2, as shown in Fig. 4. A lubricated regime was observed for both the capsule and the parenchyma (*SI Appendix*, Fig. S8), confirming that those tissue surfaces are wet by a liquid layer. Accordingly, a similar adhesion energy (0.07 ± 0.03 J/m^2) was measured when peeling the polyethylene ribbons from a water surface (Fig. 4).

In contrast, covering liver tissues with a dry PEG film for 10 min before peeling of a polyethylene ribbon leads to a remarkable 10-fold increase in adhesion energy, as shown in Fig. 4. For both the capsule and parenchyma, this change in adhesive property corresponds to a transition from a lubricated to an adhesive regime (*SI Appendix*, Fig. S8 and Movies S4 and S5). An explanation for this effect could be that, once dehydrated by the PEG membrane, the networks of biomacromolecules forming the superficial tissues become intrinsically adhesive, like the weakly cross-linked polymer networks of pressure-sensitive adhesives (PSAs) (29). As an illustration, comparable adhesion energies were obtained when peeling the polyethylene ribbons from a commercial PSA (Fig. 4).

Modeling the Role of Interfacial Fluid Transport on Hydrogel–Liver Adhesion. Our model experiments show that hydrogel-liver adhesion is strongly dependent on contact time, liver hydration, and hydrogel

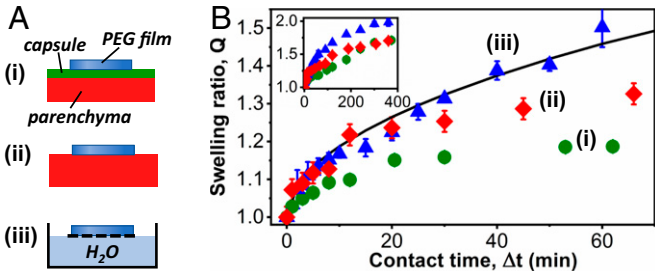

Fig. 3. Fluid transport across the hydrogel–tissue interface. (*A*) Schematic representation of swelling experiments on the liver capsule (*i*), on the liver parenchyma (*ii*), and on a water reservoir (*iii*). (*B*) Swelling ratio of PEG films as a function of contact time. Films were deposited in a dry state on the liver capsule (green circles), on the liver parenchyma (red diamonds), and on a water reservoir (blue triangles). Full line is a fit by a diffusive model of hydrogel swelling (28). *Inset* shows the same data up to long contact times.

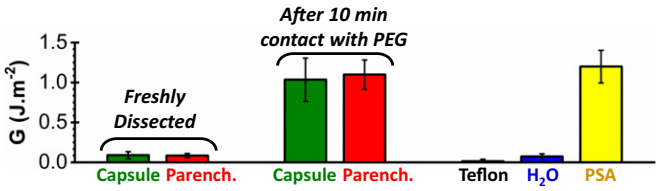

Fig. 4. Bioadhesion before and after dehydration. Adhesion energies were obtained by peeling polyethylene ribbons from the capsule (green) and parenchyma (red) of a freshly dissected liver, before and after a 10-min contact with a dry PEG film. Adhesion energies obtained by peeling the same polyethylene ribbons on Teflon (black), water (blue), and a commercial PSA (yellow) are given as a comparison (Δt = 5 min).

swelling ratio. All of these effects can be explained by a microscopic picture describing the transport processes at the tissue–hydrogel interface. For that, we consider that the water contained in tissues is distributed in two distinct phases: "free water," which is in biological fluids, and "tissue water," which is osmotically trapped in the solid tissue components, namely the cells and the extracellular matrix. In ex vivo conditions, a finite volume of free water is accessible to wet the surface of tissues, as depicted in Fig. 5*A*. For serous surfaces like the liver capsule, the basal membrane creates a rather impermeable separation from the inner tissues, and the reservoir of free water only consists in the glycocalyx layer covering the epithelium (20). For the internal surfaces of lobular organs like the liver parenchyma, the free water reservoir is composed of blood and bile, which are located in the porosities and interstitial spaces of lobules and vessels. If the liver parenchyma is exposed (e.g., after cutting), this free water quickly exudates, and a thin fluid layer wets the surface.

When a hydrogel film is applied on a tissue surface, several processes compete to take water to and out of the interface, as illustrated in Fig. 5*B*. On the one hand, the interface is drained by the swelling hydrogel, provided that it is not already swollen to equilibrium. On the other hand, water is brought to the interface from the reservoir of free fluid. In an ex vivo situation, this wetting process is driven by capillary effects, which are much faster than the swelling of the hydrogel network. For example, in the case of liver parenchyma, the capillary rise of a 10-μm-thick fluid layer to the tissue surface occurs within 0.1 ms, while it takes at least 1 s for the studied PEG hydrogels to absorb the same amount of liquid (see detailed calculation in *SI Appendix*, section 5). Consequently, a liquid film should wet the hydrogel–tissue interface as long as there is free water contained in the superficial tissues.

After a given contact time, two situations can arise. In the first situation (Fig. 5*C*), the hydrogel film could not absorb all of the free fluid reservoir. A liquid film remains at the interface, therefore preventing an intimate bonding and causing the poor adhesion observed in the lubricated regime. In the second situation (Fig. 5*D*), the volume of water absorbed by the hydrogel film exceeds the available volume of free water. The interface is thus completely drained, allowing a molecular contact, interdiffusion, and short-range interactions between the hydrogel strands and the tissue macromolecules (14). Subsequently, tissue water is extracted out of the cells or extracellular matrix in the vicinity of the interface. In this dehydrated state, the tissue resembles the highly dissipative polymer networks composing PSAs. This case leads to the observed adhesive regime.

A simple model based on this microscopic picture captures the transition between lubricated and adhesive regimes. For one unit area of interface, this model compares the volume of free water available at the interface before peeling, v_{free}, to the volume of water absorbed by the hydrogel at the time of peeling, v_{abs}. The value of v_{abs} depends on the contact time Δt, the hydrogel swelling ratio Q, and the tissue nature and water content H. It can be measured experimentally by weighing the mass of the ribbons before and after peeling. In that case, it is simply given by $v_{abs} = \Delta m/\rho A$, where Δm is the mass uptake of the ribbon after Δt, ρ is the water density, and A is the contact area.

The value of v_{free} depends on the microanatomy of the tissue surface. For the liver capsule, it can be approximated to the characteristic thickness, h_0, of the glycocalyx,

$$v_{free,\,capsule} = h_0. \qquad [1]$$

Reported values of the glycocalyx thickness vary from a few micrometers (30) to up to 60 μm (31). Hereby, we choose h_0 = 15 μm, as obtained by dividing the amount of fluid in the peritoneal coat (20 mL) (32) by its surface (1.4 m^2) (33).

For the liver parenchyma, v_{free} corresponds to the water contained in the porosities of the first layer of superficial lobules. It can be expressed as follows (see detailed calculation in *SI Appendix*, section 5):

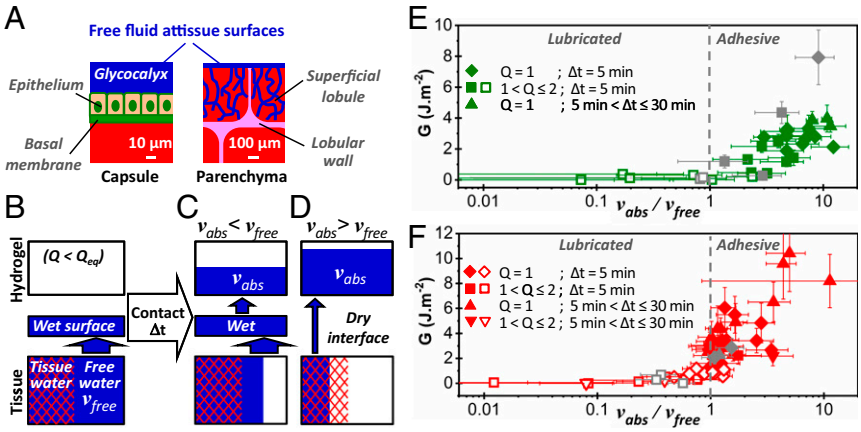

Fig. 5. Role of interfacial fluid transport on hydrogel–liver adhesion. (*A*) Schematic representation of the free fluid available to wet the surfaces of liver capsule and parenchyma. (*B*) Distribution of water in superficial liver tissues just before contact with a hydrogel. Capillary transport of free fluid ensures a rapid wetting of the tissue–hydrogel interface. Two situations arise after a given contact time: (*C*) Some free fluid remains in the tissue and wets the interface; this leads to a lubricated regime. (*D*) All of the free fluid has been absorbed, causing draining of the interface and dehydration of superficial tissues; this leads to an adhesive regime. (*E* and *F*) Adhesion energy as a function of v_{abs}/v_{free} for the (*E*) liver capsule and (*F*) parenchyma. Diamonds correspond to peelings performed with dry PEG ribbons after 5 min of contact. Different symbol shapes correspond to different values of contact time and hydrogel swelling ratio. Full and open symbols correspond to adhesive and lubricated peeling, respectively. Gray data points were obtained with modified PEG–RGD membranes. (Values chosen for calculation of v_{free}: h_0 = 15 μm, H_0 = 0.79, Φ_0 = 0.3, l_0 = 1.3 mm for freshly dissected liver, and l_0 = 1.8 mm for drained liver.)

$$v_{free,\,parenchyma} = \frac{l_0}{2}\left[1-(1-\Phi_0)\left(\frac{1-H}{1-H_0}\right)\right]\left(\frac{1-H_0}{1-H}\right)^{1/3}, \quad [2]$$

where H and H_0 are the water content of the liver in testing conditions and physiological conditions, respectively, and Φ_0 and l_0 are the average lobule porosity and diameter in physiological conditions, respectively ($H_0 = 0.79$, $\Phi_0 = 0.3$, and $l_0 =$ 1.2 mm to 1.9 mm).

The wetting state of the hydrogel–tissue interface is characterized by the dimensionless ratio v_{abs}/v_{free}. For $v_{abs}/v_{free} < 1$, the interface is still wet by free fluid at the moment of peeling: A lubricated regime should be observed. For $v_{abs}/v_{free} > 1$, the membrane has absorbed all of the free fluid, and superficial tissues are in a dehydrated state: An adhesive regime should be observed. We find these predictions to be in remarkable agreement with the experimental data, as shown in Fig. 5 *E* and *F* by plotting G as a function of v_{abs}/v_{free} for the capsule and the parenchyma. Those graphs represent all of the data obtained from peeling experiments with various contact times, tissue hydration, and hydrogel swelling ratio. For both the capsule and parenchyma, a transition from lubricated to adhesive peeling occurs around a value of $v_{abs}/v_{free} = 1$. In the adhesive regime, the ratio v_{abs}/v_{free} also reflects the level of tissue dehydration: The higher it is, the more dehydrated the tissues are. Accordingly, we find that adhesion energy increases with tissue dehydration, as in the case of mucoadhesion (13).

In the adhesive regime, the strength of adhesion due to binding and interdiffusion across the interface should strongly depend on the chemistry and dynamics of the hydrogel network (14). To illustrate this point, peeling experiments were performed with membranes containing grafted tripeptide Arg-Gly-Asp (RGD) to enhance adhesion to cell membranes (*SI Appendix*, section 2). These PEG–RGD membranes have the same swelling behavior as PEG membranes (*SI Appendix*, Fig. S2). For both the capsule and the parenchyma, a transition from lubricated to adhesive regime occurs at $v_{abs}/v_{free} = 1$ like for the PEG without RGD, as shown in Fig. 5 *E* and *F*. In the adhesive regime, the presence of RGD causes a significant increase in adhesion to the capsule but not to the parenchyma. This is consistent with differences in the nature of the tissues. Indeed, the density in membrane adhesion proteins is expected to be much larger at the surface of the capsule than at the cut surface of the parenchyma where cells are damaged and covered with blood proteins. Most interestingly, a fourfold increase in adhesion energy is obtained on the capsule for v_{abs}/v_{free} going from 1.5 to 10, which confirms the strong enhancement of adhesion caused by local dehydration.

Design of Improved Bioadhesive Hydrogels and in Vivo Adhesion. Our findings suggest that improved bioadhesive performances should be obtained using superabsorbent membranes having enhanced swelling kinetics and absorption capacity. We verified this hypothesis by comparing the bioadhesion of the model PEG films with that of superabsorbent meshes of Oxidized Regenerated Cellulose (ORC). This latter system is used as a hemostat in surgery (34). The presence of ether oxygens as well as hydroxy and carboxylic groups in ORC suggests the possibility of hydrogen bonding with other biomolecules, as already reported to explain its hemostatic properties (35).

ORC meshes swell much faster than PEG films, with an equilibrium swelling ratio of 3.5 reached in less than 1 min in water (*SI Appendix*, Fig. S9). When deposited at the surface of liver parenchyma or capsule, 150-μm-thick ORC meshes quickly drain the interface by capillary transport of free water, and the criterion for adhesive contact ($v_{abs}/v_{free} > 1$) is reached within less than 1 min (Fig. 6*A*). For longer contact times (>5 min), a slower swelling regime takes place, corresponding to extraction of trapped water from capsule cells and deeper tissues. Between these two regimes (1 min to 5 min), a small decay in membrane swelling is observed, which we attribute to water evaporation from the ORC mesh. Ex vivo peeling confirms that these superabsorbent meshes strongly adhere to the liver capsule and parenchyma when they are deposited in a dry state (*SI Appendix*, Fig. S10). For a 5-min contact on a freshly dissected liver with moderate hydration ($H = 76$ wt%), the adhesion energy of dry ORC meshes to the parenchyma (capsule) is 14 (1.8) times greater than that of 1-mm-thick dry PEG films (Fig. 6 *B* and *C*). The stronger adhesion energy obtained with ORC may arise from a higher density or strength of the binding functions as well as from dissipative friction caused during the deformation of the fibrous ORC mesh. Conversely, poor adhesion and lubricated regimes were obtained when the ORC meshes were deposited on a very hydrated parenchyma ($H = 81$ wt%) (Fig. 6*B*) or were swollen to equilibrium before contact (Fig. 6*C*).

While the fluid content of ex vivo tissues is limited and static, in vivo tissues are continuously perfused with biological fluids. Draining of hydrogel–tissue interfaces and establishment of a durable adhesive contact should therefore be more difficult to achieve in vivo than ex vivo. For the liver parenchyma, surface bleeding is so strong (10 $\mu L \cdot cm^{-2} \cdot min^{-1}$ to 100 $\mu L \cdot cm^{-2} \cdot min^{-1}$) (36) that

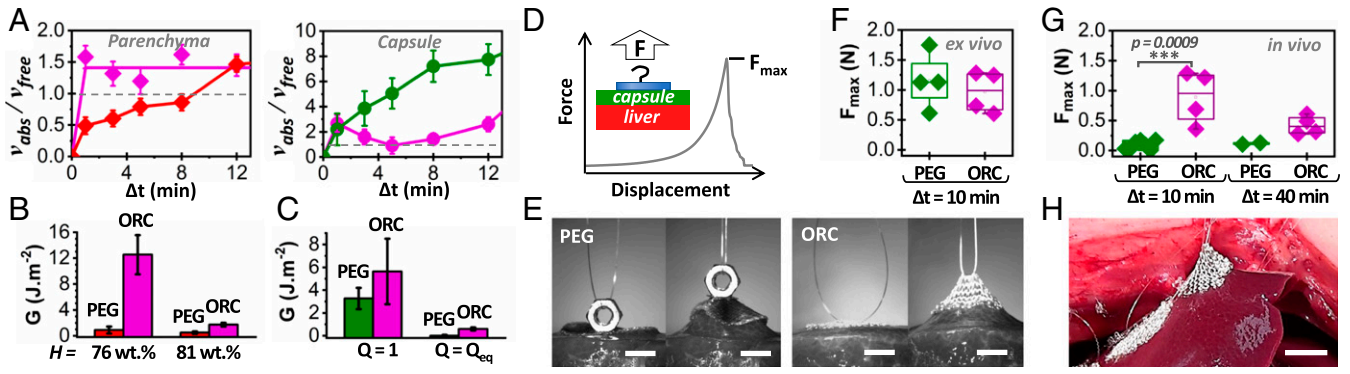

Fig. 6. Adhesion of superabsorbent membranes and in vivo adhesion. (*A*) Ratio v_{abs}/v_{free} as a function of contact time for ORC meshes (violet symbols) deposited on the parenchyma and capsule of a freshly dissected liver ($H = 77.9$ wt%). Data are compared with those for PEG films in the same conditions (red diamonds and green circles). (*B*) Adhesion energies obtained by peeling ORC meshes and PEG ribbons from liver parenchyma with different water content H. (*C*) Adhesion energies obtained by peeling ORC meshes and PEG ribbons at different levels of initial swelling from the liver capsule. (*D*) Schematic representation of the tack-like protocol for in vivo adhesion testing and typical force–displacement curve starring F_{max}, the maximum detachment force. (*E*) Snapshots of tack experiments performed ex vivo on freshly dissected liver capsules with PEG membrane and ORC meshes. (Scale bar: 5 mm.) (*F*) Maximum detachment force of PEG films and ORC meshes obtained ex vivo on the liver capsule after 10-min contact time. (*G*) Maximum detachment force of PEG films and ORC meshes obtained in vivo on the liver capsule after 10- and 40-min contact times. (*H*) Picture of an in vivo tack experiment displaying the lifting of an entire hepatic lobe during the detachment of an ORC mesh after 10-min contact on the liver capsule. (Scale bar: 10 mm.)

membrane swelling is unlikely to drain the interface and create adhesion, unless hemostatic processes are activated. For the liver capsule, however, exudation of water across the basal membrane is moderate (0.05 $\mu L \cdot cm^{-2} \cdot min^{-1}$ to 0.5 $\mu L \cdot cm^{-2} \cdot min^{-1}$) (37, 38). An adhesive regime should be attainable with the swelling kinetics of hydrogel membranes. In vivo adhesion experiments were performed on the liver capsule of anesthetized pigs under laparotomy ($n = 2$) (see detailed protocols in *SI Appendix*, section 6). For that, a portable tack-like protocol was devised that measures the maximum force required to detach a hydrogel membrane by pulling perpendicularly to the capsule surface, as depicted in Fig. 6*D*. Disks with a diameter of 1.6 cm of both dry PEG films and dry ORC meshes were deposited onto the liver capsule. Pressure was applied digitally for 30 s, and the films were detached after a given contact time. When this tack protocol was performed on ex vivo tissues for a 10-min contact time, both PEG films and ORC meshes strongly adhered to the liver capsule, with detachment forces of the order of 1.1 ± 0.4 N (Fig. 6*E*) and large tissue deformation (Fig. 6*F* and Movies S6 and S7). For in vivo experiments (Fig. 6*G*), the detachment force of the dry PEG films was 10 times lower (0.09 ± 0.07 N) than ex vivo. A much better resistance to in vivo tissue hydration was obtained with ORC meshes. After a 10-min contact, the detachment force was maintained close to that of ex vivo conditions (0.9 ± 0.4 N), and a twofold decrease was observed after 40 min of contact. As an illustration of the practical relevance of these adhesives, the in vivo adhesion of the ORC patches was strong enough to lift the liver lobes (Fig. 6*H* and Movie S8).

In conclusion, these results demonstrate that interfacial fluid transport is central to the establishment of adhesion between hydrogels and internal tissues. While the current study concentrates on liver, the concepts and predictions are most likely applicable to many other internal organs having similar serous or lobular histology, like kidney, gall bladder, or pancreas. These findings provide insight into the design of bioadhesion tests. In particular, the reported experiments and model indicate that the monitoring of tissue hydration and interfacial liquid exchanges greatly improves the discriminating power of bioadhesion measurements. Moreover, the possibility of imparting adhesiveness to tissues and enhancing hydrogel adhesion through local dehydration brings forward a lever to tailor the fixation of hydrogel-based devices and implants. Our ex vivo and in vivo results show that this effect can be sustained for at least 1 h, which is of immediate interest for bioadhesive applications in perioperative conditions. More generally, combining this understanding with other bioadhesive approaches using specific binding functions (7–9, 17, 19), adsorption effects (11, 18), or roughness and mechanical anchoring (10) opens a route for more functional strategies where adhesion strength and durability can be adjusted to the targeted applications and to the microanatomy of the tissues of interest.

Materials and Methods

Details about the hydrogel synthesis, the tissue preparation, the characterization of fluid transport, and the protocols for ex vivo and in vivo adhesion testing are given in *SI Appendix, SI Materials and Methods*. Calculations to model interfacial fluid transport are also described in detail in *SI Appendix, SI Materials and Methods*.

ACKNOWLEDGMENTS. We thank L. Leibler for initiating this research and for stimulating discussions on hydrogel adhesion; E. Vibert and N. Golse for discussions on surgical adhesives; and F. Tournilhac for the characterization of RGD grafting. Technological support from the Institut P-G de Gennes Program ANR-10-EQPX-34 as well as financial support from Program Paris Sciences et Lettres Chimie 2014 Grant HemoSoftChem, MINES ParisTech, ESPCI Paris, and the Fonds Charpack are acknowledged.

1. Lutolf MP, et al. (2003) Synthetic matrix metalloproteinase-sensitive hydrogels for the conduction of tissue regeneration: Engineering cell-invasion characteristics. *Proc Natl Acad Sci USA* 100:5413–5418.
2. Kim KD, Wright NM (2011) Polyethylene glycol hydrogel spinal sealant (DuraSeal spinal sealant) as an adjunct to sutured dural repair in the spine: Results of a prospective, multicenter, randomized controlled study. *Spine* 36:1906–1912.
3. Peppas NA, Hilt JZ, Khademhosseini A, Langer R (2006) Hydrogels in biology and medicine: From molecular principles to bionanotechnology. *Adv Mater* 18: 1345–1360.
4. Urban GA, Weiss T (2009) Hydrogels for biosensors. *Hydrogel Sensors and Actuators*, eds Gerlach G, Arndt K-F (Springer, Berlin), pp 197–220.
5. Lauto A, Mawad D, Foster LJR (2008) Adhesive biomaterials for tissue reconstruction. *J Chem Technol Biotechnol* 83:464–472.
6. Mehdizadeh M, Yang J (2013) Design strategies and applications of tissue bioadhesives. *Macromol Biosci* 13:271–288.
7. Artzi N, Shazly T, Baker AB, Bon A, Edelman ER (2009) Aldehyde-amine chemistry enables modulated biosealants with tissue-specific adhesion. *Adv Mater* 21:3399–3403.
8. Liu X, Zhang Q, Gao G (2017) Bioinspired adhesive hydrogels tackified by nucleobases. *Adv Funct Mater* 27:1703132.
9. Shin J, et al. (2015) Tissue adhesive catechol-modified hyaluronic acid hydrogel for effective, minimally invasive cell therapy. *Adv Funct Mater* 25:3814–3824.
10. Yang SY, et al. (2013) A bio-inspired swellable microneedle adhesive for mechanical interlocking with tissue. *Nat Commun* 4:1702.
11. Meddahi-Pellé A, et al. (2014) Organ repair, hemostasis, and in vivo bonding of medical devices by aqueous solutions of nanoparticles. *Angew Chem Int Ed Engl* 53:6369–6373.
12. Annabi N, et al. (2014) Surgical materials: Current challenges and nano-enabled solutions. *Nano Today* 9:574–589.
13. Mortazavi SA, Smart JD (1993) An investigation into the role of water movement and mucus gel dehydration in mucoadhesion. *J Controlled Release* 25:197–203.
14. Smart JD (2005) The basics and underlying mechanisms of mucoadhesion. *Adv Drug Deliv Rev* 57:1556–1568.
15. Borde A, Bergstrand A, Gunnarsson C, Larsson A (2010) Osmotic-driven mass transport of water: Impact on the adhesiveness of hydrophilic polymers. *J Colloid Interface Sci* 341:255–260.
16. Caccavo D, Lamberti G, Cascone S, Barba AA, Larsson A (2015) Understanding the adhesion phenomena in carbohydrate-hydrogel-based systems: Water up-take, swelling and elastic detachment. *Carbohydr Polym* 131:41–49.
17. Li J, et al. (2017) Tough adhesives for diverse wet surfaces. *Science* 357:378–381.
18. Roy CK, et al. (2015) Self-adjustable adhesion of polyampholyte hydrogels. *Adv Mater* 27:7344–7348.
19. Ryu JH, et al. (2011) Catechol-functionalized chitosan/pluronic hydrogels for tissue adhesives and hemostatic materials. *Biomacromolecules* 12:2653–2659.
20. van Baal JOAM, et al. (2017) The histophysiology and pathophysiology of the peritoneum. *Tissue Cell* 49:95–105.
21. Sear J (1992) Anatomy and physiology of the liver. *Baillieres Clin Anaesthesiol* 6:697–727.
22. White EG (1939) Some observations on the liver of the pig: The hepatic lobule and liver cell during post-natal growth. *J Anat* 73:365–386.1.
23. Kim J, Ahn B, De S, Srinivasan MA (2008) An efficient soft tissue characterization algorithm from in vivo indentation experiments for medical simulation. *Int J Med Robot* 4:277–285.
24. Huang L, Nagapudi K, Apkarian RP, Chaikof EL (2001) Engineered collagen-PEO nanofibers and fabrics. *J Biomater Sci Polym Ed* 12:979–993.
25. Knowles DB, et al. (2015) Chemical interactions of polyethylene glycols (PEGs) and glycerol with protein functional groups: Applications to effects of PEG and glycerol on protein processes. *Biochemistry* 54:3528–3542.
26. Sheth SR, Leckband D (1997) Measurements of attractive forces between proteins and end-grafted poly(ethylene glycol) chains. *Proc Natl Acad Sci USA* 94:8399–8404.
27. Kendall K (1975) Thin-film peeling–Elastic term. *J Phys D Appl Phys* 8:1449–1452.
28. Ritger PL, Peppas NA (1987) A simple equation for description of solute release I. *J Controlled Release* 5:23–36.
29. Shull KR (2002) Contact mechanics and the adhesion of soft solids. *Mater Sci Eng Rep* 36:1–45.
30. Servais AB, et al. (2017) Structural heteropolysaccharide adhesion to the glycocalyx of visceral mesothelium. *Tissue Eng Part A* 24:199–206.
31. Wilson RB (2017) Changes in the coelomic microclimate during carbon dioxide laparoscopy: Morphological and functional implications. *Pleura Peritoneum* 2: 17–31.
32. Brady M, Mahoney E (2015) Peritoneal cavity. *Current Diagnosis & Treatment: Surgery*, ed Doherty GM (McGraw-Hill, New York), 14th Ed, pp 498–513.
33. Albanese AM, et al. (2009) Peritoneal surface area: Measurements of 40 structures covered by peritoneum: Correlation between total peritoneal surface area and the surface calculated by formulas. *Surg Radiol Anat* 31:369–377.
34. Ferretti L, Qiu X, Villalta J, Lin G (2012) Efficacy of BloodSTOP iX, surgicel, and gelfoam in rat models of active bleeding from partial nephrectomy and aortic needle injury. *Urology* 80:1161.e1–1161.e6.
35. Ryšavá J, et al. (2003) Surface interactions of oxidized cellulose with fibrin(ogen) and blood platelets. *Sens Actuators B Chem* 90:243–249.
36. Greenway CV, Lautt WW (2010) Hepatic circulation. *Comprehensive Physiology* (John Wiley, New York), pp 1519–1564.
37. Cochrane SM, Byrne JC, Robinson GB (1997) The permselectivity of glomerular basement membrane can be compromised by glycation or by exposure to low levels of hypochlorite. *Biochim Biophys Acta* 1361:217–228.
38. Fisher RF (1982) The water permeability of basement membrane under increasing pressure: Evidence for a new theory of permeability. *Proc R Soc Lond B Biol Sci* 216:475–496.